

High Pressure Pyrolysis of Toluene. 2. Modeling Benzyl Decomposition and Formation of Soot Precursors

R. Sivaramakrishnan,[†] Robert S. Tranter,[‡] and K. Brezinsky^{*,†}

Departments of Mechanical & Industrial Engineering, University of Illinois at Chicago, Chicago, Illinois 60607, and Chemistry Division, Argonne National Laboratory, Argonne, Illinois 60439

Received: February 8, 2006; In Final Form: May 10, 2006

The pyrolysis of toluene, the simplest methyl-substituted aromatic molecule, has been studied behind reflected shock waves using a single pulse shock tube. Part 1 in this two-part series focused on the high-pressure experimental results and the high-pressure limiting rate coefficients for the primary steps in toluene decomposition. The present work focuses on the modeling of benzyl decomposition and the growth of key soot precursors (C_2H_2 , C_4H_2 , C_8H_6 , and indene) from toluene pyrolysis with 81 among the 262 reactions in the detailed toluene model representing the chemistry that describes the formation and decomposition of these species. Feasible pathways for benzyl decomposition as well as phenylacetylene and indene formation have been tested. The simulations also show very good agreement with the single pulse shock tube profiles for the growth of key soot precursors such as C_2H_2 , C_4H_2 , C_8H_6 , and indene.

Introduction

The high temperature pyrolysis of toluene has been an area of intense research in the combustion kinetics community over the past decade because of its abundance in commercial fuels. A brief summary of prior studies have mentioned in part I in this series.¹ Among the experimental studies only the Knudsen cell–mass spectrometry study by Smith^{2,3} and the shock tube studies by Pamidimukkala et al.⁴ and Colket and Seery⁵ attempted to characterize the intermediates that form during the high-temperature pyrolysis of toluene. Pamidimukkala et al.⁴ performed experiments in a shock tube coupled to a time-of-flight mass spectrometer. Their experiments were performed at pressures from 0.2 to 0.5 atm over the temperature range 1550–2200 K and the primary species observed in these experiments were C_2H_2 , C_4H_2 , and CH_4 . Colket and Seery⁵ used a single pulse shock tube over the temperature range 1200–1850 K at pressures of 10 atm to obtain species profiles for the dominant small hydrocarbon intermediates along with a large number of single ring aromatics and multi ring PAHs. There are no other reported measurements of stable species profiles over a wide range of temperatures especially at high pressures relevant to practical combustion.

Part 1 in this series¹ focused on modeling key species profiles ($C_6H_5CH_3$, CH_4 , C_6H_6) from our HPST experiments coupled with H atom shock-tube–ARAS data from Braun-Unkhoff et al.⁶ and Eng et al.⁷ and the results of recent theoretical calculations by Klippenstein et al.⁸ to extract accurate high pressure limit primary rate coefficients and their high temperature branching ratios in toluene decomposition. However, the dominant intermediates from the pyrolysis of toluene such as acetylene, diacetylene, benzyl, phenylacetylene, and indene represent key soot precursors and consequently the description of the chemistry that leads to the formation and destruction of these species at high temperatures is critical to obtaining a

fundamental understanding of the soot formation process. The soot precursor species profiles from the current experiments represent key validation targets for the pyrolytic steps in large combustion models and consequently in this work we have tested mechanistic routes that describe aromatics growth and consumption on the basis of the HPST data.

Modeling Acetylene Formation and Benzyl Decomposition

The current high-pressure toluene pyrolysis experiments yielded C_2H_2 which was the most dominant intermediate with mole fractions >100 ppm. C_2H_2 starts to build up in significant amounts at temperatures below 1400 K (see Figures 2 and 3 in part 1 of this series) which is definitive evidence for its formation from the decomposition of the benzyl radical,⁵ albeit not via a direct unimolecular step. The formation of C_2H_2 from benzyl has been a source of uncertainty with multiple mechanisms proposed by several investigators. Jones et al.⁹ have performed ab initio calculations to evaluate the contributions/importance of the several channels for benzyl decomposition. They concluded that direct ring opening and the isomerization to a 6-methylenebicyclo[3.1.0]hex-3-en-2-yl [MBH] intermediate were the most energetically favorable pathways. They were able to extract rate constants for the two channels using canonical TST. In prior work on the decomposition of benzyl radicals, Braun-Unkhoff et al.¹⁰ concluded that over the temperature range 1400–1700 K benzyl dissociates primarily to H atoms and an unknown product. To explain the H atom formation from their benzyl decomposition experiments, Hippler et al.¹¹ have proposed an alternate sequence of steps involving the formation of bibenzyl from which H atoms are removed to eventually form stilbene. In more recent work Oehlschlaeger et al.¹² have performed experiments behind reflected shock waves and have detected benzyl via UV laser absorption. Oehlschlaeger et al.¹² have concluded that the primary decomposition channel for benzyl decay is via the formation of a C_7H_6 species on the basis of the experiments by Frochtenicht et al.¹³ who observed a C_7H_6 and H atom fragment in their photoin-

* Corresponding author. E-mail: Kenbrez@uic.edu.

[†] University of Illinois at Chicago.

[‡] Argonne National Laboratory.

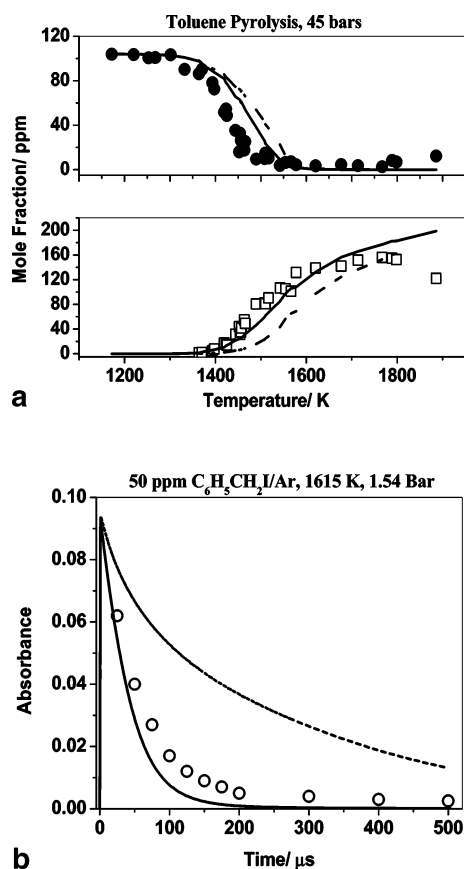


Figure 1. (a) HPST profiles: (●) $C_6H_5CH_3$; (□) C_2H_2 ; (---) detailed model with benzyl decomposition pathway in Table 1; (---) detailed model with global steps for benzyl decay from Colket and Seery.⁵ (b) Benzyl absorbance profiles: (○) $C_6H_5CH_2$ absorbance data from Figure 2;¹² (---) detailed model with benzyl decomposition pathway in Table 1; (---) detailed model with global steps for benzyl decay from Colket and Seery.⁵

duced benzyl decomposition experiments in a molecular beam. The rate coefficients extracted for benzyl decay by Oehlschlaeger et al.¹² agrees with the measurements of Braun-Unkhoff et al.¹⁰ and Hippler et al.¹¹ despite the different mechanistic interpretations offered by these authors. Although a C_7H_6 fragment was detected by Frochtenicht et al.¹³ in their experiments, the molecular structure of the C_7H_6 fragment has not been conclusively determined. Braun-Unkhoff et al.¹⁰ have proposed that benzyl decomposition is preceded by benzyl isomerization which leads to the C_7H_6 fragment (a cyclic species—acetylcyclopentadiene) and this pathway has been shown through the ab initio computations by Jones et al.⁹ to be a dominant benzyl decomposition channel. Using the information from the calculations of Jones et al.⁹ as well as the conclusions of Braun-Unkhoff et al.,¹⁰ Laskin and Lifshitz¹⁴ included a series of steps to describe benzyl decomposition in their shock tube study on the thermal decomposition of indene. The sequence of steps not only accounts for H atom formation but also explains C_2H_2 production from benzyl. The sequence of steps along with the associated rate parameters is shown below in Table 1.

The sequence of steps shown in Table 1 was incorporated into our model to better describe benzyl dissociation. Figure 1a depicts the acetylene and toluene profiles which have been obtained for the higher pressure data set at 45 bar. With the detailed steps in Table 1 included the model fails to reproduce the C_2H_2 profile for the 45 bar data set with deviations varying from a factor of 3 and higher at temperatures <1400 K to a

TABLE 1: Alternate Benzyl Decomposition Pathways (Units in cm^3 , s, mol, cal)

reaction	A	E_a
$C_6H_5CH_2 \rightarrow C_5H_5CCH_2$	2.00×10^{14}	75 000
$C_5H_5CCH_2 \rightarrow C_5H_5C_2H + H$	3.20×10^{15}	34 000
$C_5H_5C_2H + H \rightarrow C_5H_5 + C_2H_2$	5.00×10^{14}	0
$C_6H_5CH_2 \rightarrow 1-C_7H_7$	1.20×10^{16}	97 000
$1-C_7H_7 \rightarrow 1-C_5H_5 + C_2H_2$	1.00×10^{14}	35 000

factor of 2 at 1600 K. Similar trends are observed for the lower pressure 27 bar data set. The failures of the model are primarily due to barriers >90 kcal/mol that need to be overcome to form acetylene via both the MBH pathway and the ring opening pathway. The model also significantly underpredicts the toluene decay when using the benzyl decomposition mechanism in Table 1. We have also simulated the absorption profiles reported by Oehlschlaeger et al.¹² Oehlschlaeger et al.¹² have reported absorption profiles for only one experiment at 1615 K and 1.54 bar. They have used dilute mixtures (50 ppm) of benzyl iodide (as benzyl precursor) in argon. To accurately reflect their experiments we have compared our model predictions for the decay of benzyl to the contributions to absorbance from benzyl alone (reported as a dot-dot-dashed line in Figure 2 of their paper). Apart from the sequence of steps in Table 1 we have also included the reactions $C_6H_5CH_2I \rightarrow C_6H_5CH_2 + I$ and its reverse reaction with rate parameters as reported by Oehlschlaeger et al.¹² Figure 1b shows the comparisons made by the model to the experimental benzyl absorption profile. The sequence of steps in Table 1 severely underpredicts the experimental trends over the entire time scale (up to 500 μs). In the absence of lower energy pathways and rigorous high level ab initio calculations we have replaced the benzyl dissociation steps in Table 1 by two overall reactions for the decomposition of the benzyl radical,

Global Steps for Benzyl Decomposition (Units in cm^3 , s, mol, cal)

reaction	A	n	E_a
$C_6H_5CH_2 \rightarrow C_5H_5 + C_2H_2$	6.03×10^{13}	0	70 000
$C_6H_5CH_2 \rightarrow C_4H_4 + H_2CCCH$	2.00×10^{14}	0	83 600

(see Supporting Information Table ST2 in part 1 of this series for rate parameters) with the rate parameters suggested by Colket and Seery.⁵ Colket and Seery derived their rate parameters from modeling acetylene profiles from toluene pyrolysis experiments as well as in mixtures with cyclopentadiene/acetylene. Adopting these global steps/rate parameters provides an excellent agreement with our measured acetylene profiles as seen in Figure 1a. Acetylene is produced primarily from the two steps $C_6H_5CH_2 \rightarrow C_5H_5 + C_2H_2$ [rate parameters from ref 5] and $C_5H_5 \rightarrow H_2CCCH + C_2H_2$ [rate parameters from ref 15]. The model with the global benzyl decomposition steps also shows reasonable agreement with the benzyl absorbance profiles as seen in Figure 1b especially at short time scales <100 μs . It is clear from the current modeling exercise that the decomposition of benzyl is far from well characterized. We have attempted to explain the benzyl decay and acetylene formation by global steps. However it is very likely that benzyl decomposition involves the sequence of steps as in Table 1 as well as direct ring rupture. However more detailed experiments that attempt to trap the intermediates that result from benzyl pyrolysis in combination with higher level ab initio techniques and more sophisticated kinetic theories than those utilized in the Jones et al.⁹ study are required to shed light on the actual mechanistic processes by which benzyl decays as well as their associated rate parameters.

Soot Precursors: Modeling Phenylacetylene and Indene Profiles

We were able to obtain profiles for C_8H_6 (phenylacetylene) and C_9H_8 (indene) among the group of smaller aromatics. The low fuel mole fractions used in this study inhibit the detection of species larger than indene although the spectrum of intermediates produced during toluene pyrolysis is rich with profiles of PAH's as large as pyrene found in prior studies.⁵ Phenylacetylene and indene, the two key small aromatics that lead to soot, were observed in small amounts on the order of 2 ppm in the current experiments. To model the formation and consumption of these species we have assembled a series of reactions with rate parameters based on literature recommendations.

The dominant route for phenylacetylene formation is via the popular HACA (hydrogen abstraction acetylene addition) mechanism^{16,17} by which $C_6H_5 + C_2H_2 \rightarrow C_8H_6 + H$. There have been a number of experimental studies on the reaction between C_6H_5 and C_2H_2 which have been summarized in a recent computational study by Tokmakov and Lin.¹⁸ Tokmakov and Lin¹⁸ have used high level ab initio techniques (G2M method) to probe the potential energy surface for the reaction between C_6H_5 and C_2H_2 . Apart from the direct route forming $C_8H_6 + H$, $C_6H_5 + C_2H_2$ primarily forms a stabilized adduct C_6H_5CHCH (2-phenylvinyl) that subsequently dissociates to $C_8H_6 + H$ and also a number of other cyclic intermediates. Tokmakov and Lin¹⁸ have used a combined RRKM/master equation analysis to derive rate coefficients for the formation of stabilized adducts (such as C_6H_5CHCH) and their subsequent dissociation and isomerization reactions. They concluded that at combustion temperatures the favored product for $C_6H_5 + C_2H_2$ is C_8H_6 . This is in line with an earlier computational study by Richter et al.¹⁹ who used DFT techniques in combination with a chemical activation analysis using QRRK theory to derive rate coefficients for the sequence $C_6H_5 + C_2H_2 \rightarrow C_6H_5CHCH \rightarrow C_8H_6 + H$. We have used the experimental rate by Heckmann et al.²⁰ for the reaction $C_6H_5 + C_2H_2 \rightarrow C_8H_6 + H$ in combination with the recommendations of Tokmakov and Lin¹⁸ for the sequence $C_6H_5 + C_2H_2 \rightarrow C_6H_5CHCH \rightarrow C_8H_6 + H$ in our model. Table ST2 in the Supporting Information in part 1 of this two-part work outlines the sequence of steps (reactions 193–197) used to describe the formation of C_8H_6 .

Despite being a key combustion intermediate and present in significant amounts in flames²¹ there are very limited thermal studies on the formation/decomposition of indene (C_9H_8), which represents the smallest five and six membered ring aromatic. The decomposition of indene has been studied by Laskin and Lifshitz¹⁴ in their single pulse shock tube and the decomposition has been shown to proceed via the formation of an indanyl radical (C_9H_9). Lindstedt et al.²¹ in their review have outlined the mechanistic routes that can form indene. The three main channels involve

- A. phenyl + allene/propyne ($C_6H_5 + C_3H_4 \rightarrow C_9H_9 \rightarrow C_9H_8 + H$)
- B. benzyl + acetylene ($C_6H_5CH_2 + C_2H_2 \rightarrow C_9H_9 \rightarrow C_9H_8 + H$)
- C. phenyl + propargyl ($C_6H_5 + C_3H_3 \rightarrow C_9H_8$)

They have proposed a series of steps involving the formation of C_9H_9 isomers that eventually cyclize to form indene. Group contribution methods were used to estimate the thermochemistry for the C_9H_9 intermediates and in the absence of experimental/

computational studies estimates were made for reaction rate coefficients for the channels. After their review, channels A and B have been investigated computationally in a series of papers by Vereecken et al.^{22–24} High level coupled cluster (CC) and quadratic configuration interaction (QCI) methods were used to obtain the potential energy surface in conjunction with an RRKM-Master equation analysis to obtain temperature/pressure dependent product distributions for channels A and B. We have assimilated the information provided by Lindstedt et al.²¹ and Vereecken et al.^{22–24} and assembled a model involving a series of elementary steps that form C_9H_9 isomers that eventually cyclize to indene. Vereecken et al.^{22–24} in their study have not provided channel specific rate constants except for the entrance channels for the reactions between $C_6H_5 + AC_3H_4$, $C_6H_5 + PC_3H_4$ and $C_6H_5CH_2 + C_2H_2$. Consequently we have utilized their barrier heights (E_0) and using a simple correlation we have set the activation energies E_a to $E_0 + MRT$ (M : molecularity of the reaction).²⁵ The preexponential frequency factors were either based on Lindstedt's estimates or estimates based on relative entropies for the C_9H_9 species. Table ST2, in the Supporting Information in part 1 of this two-part work incorporates the mechanism used to describe the formation of indene (reactions 225–255).

The species identities are the same as that used by Lindstedt et al.²¹ and Vereecken et al.^{23,24} and are depicted in the Supporting Information, Table ST1. Parts a and b of Figure 2 depict the model predictions for phenylacetylene and indene for the 27 and 45 bar experiments, respectively. The sequence of steps in Table ST2, from part 1, describes the buildup of phenylacetylene (see Figure 2, parts a and b) fairly adequately at temperatures < 1470 K beyond which the experiments show a decay which is not captured by the model because of the lack of adequate decomposition steps for the C_8H_6 forming larger PAHs. We have restricted the model to depict only a few steps leading to the formation of naphthalene ($C_{10}H_8$) in the absence of species profiles for $C_{10}H_8$ and larger species. Reasonably good agreement is also obtained for the indene experimental profiles using the sequence of steps outlined in Table ST2, in part 1 (reactions 225–255). Figure 3 depicts sensitivity analyses that were performed for C_8H_6 and C_9H_8 concentrations for a 45 bar experiment at 1509 K. The reactions between C_6H_5 and C_2H_2 forming C_6H_5CHCH adduct as well as C_8H_6 directly are the most sensitive reactions in the model for phenylacetylene concentrations. In the case of indene the two most sensitive reactions are $C_6H_5CH_2 + C_2H_2 = p\text{-}C_9H_9$ as well as decomposition of $c\text{-}C_9H_9$ to indene. The reactions between C_6H_5 and PC_3H_4 and AC_3H_4 do not appear to be sensitive in this case probably due to the relatively low concentrations of these species in comparison to the large amounts of $C_6H_5CH_2$ and C_2H_2 which are formed in the current toluene experiments.

Rates of production analyses were performed for the three major intermediates C_2H_2 , C_8H_6 and C_9H_8 for an example shock at $T = 1509$ K and $P = 45$ bar. The majority of C_2H_2 (82%) is produced in equal amounts by the two reactions $C_6H_5CH_2 = C_5H_5 + C_2H_2$ and $C_5H_5 = H_2CCCH + C_2H_2$ with C_5H_5 being formed exclusively via $C_6H_5CH_2 = C_5H_5 + C_2H_2$. The benzyl radical thereby appears to be the dominant source for the C_2H_2 produced specifically in the lower temperature range of the current experiments [1200–1500 K] with contributions from other species such as C_6H_5 beginning to be dominant at the higher temperatures (> 1600 K). Figure 4 illustrates the contributions from various channels to the production of acetylene at temperatures 1300, 1500, and 1700 K. Up to 85% of C_8H_6 is formed from the two channels $C_6H_5 + C_2H_2 \rightarrow C_8H_6 + H$ (54%)

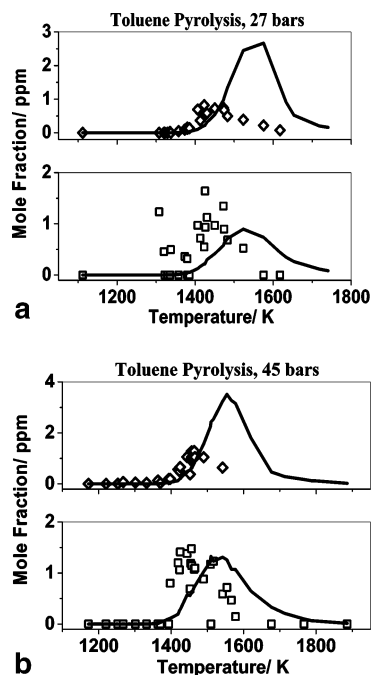


Figure 2. (a) HPST profiles at 27 bar: (\diamond) C_8H_6 ; (\square) C_9H_8 ; (—) detailed model with steps from Table ST2, part 1. (b) HPST profiles at 45 bar: (\diamond) C_8H_6 ; (\square) C_9H_8 ; (—) detailed model with steps from Table ST2, part 1.

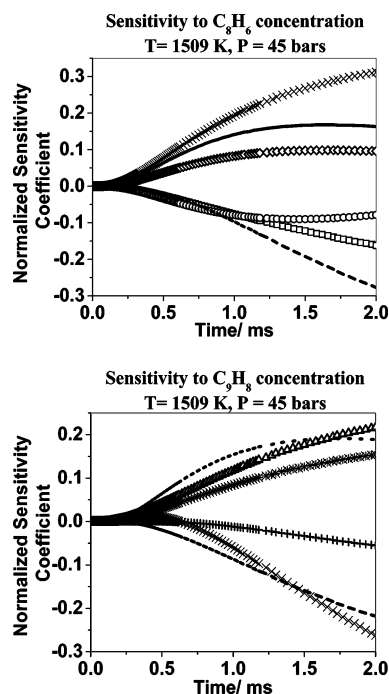


Figure 3. Sensitivity analyses: (—) $C_6H_5CH_2 + H_2CCCH = C_{10}H_8 + H + H$; (\times) $C_6H_5CH_2 = C_6H_5 + C_2H_2$; (—) $C_6H_5 + C_2H_2 = C_8H_6 + H$; ($*$) $C_6H_5CH_2 + C_2H_2 = p\text{-}C_9H_9$; (\square) $C_4H_3 = C_4H_2 + H$; (\diamond) $C_6H_5CHCH = C_8H_6 + H$; (+) $C_6H_5CH_3 + H = C_6H_6 + CH_3$; (\circ) $C_6H_6 = C_6H_5 + H$; (\cdots) $C_6H_5CH_3 + H = C_6H_5CH_2 + H_2$; (Δ) $c\text{-}C_9H_9 = C_9H_8 + H$.

and $C_6H_5 + C_2H_2 \rightarrow C_6H_5CHCH$ (41%). These reactions are not only the two most dominant but also the most sensitive reactions as seen in Figure 3. The majority of the indene (90%) is formed by the reaction $c\text{-}C_9H_9 \rightarrow C_9H_8 + H$ due to the large amounts of C_2H_2 and $C_6H_5CH_2$ present in these experiments with the remaining 10% produced by $s\text{-}C_9H_9 \rightarrow C_9H_8 + H$. The only other species formed in significant amounts ~ 1 ppm, apart from diacetylene which is formed in amounts > 20 ppm,

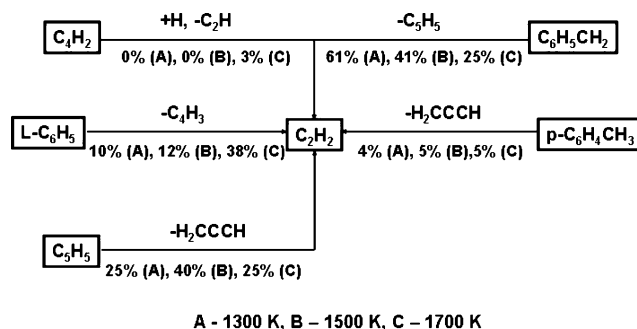


Figure 4. Acetylene Rates of Production, 45 bar.

are styrene, xylene, ethylbenzene, and vinylacetylene. The detailed model [See supplementary information Table ST2 in part 1 in this series on toluene pyrolysis for detailed model] includes reactions for the formation and consumption of these species.

Figure 5 depicts the model predictions for C_4H_2 , C_4H_4 , C_8H_8 , p -xylene, and ethylbenzene. The model is able to predict the C_4H_2 concentrations fairly accurately at temperatures < 1550 K. At higher temperatures the model over predicts the C_4H_2 formed in contrast to the experiments which depict a decay. However given the uncertainties with regard to the diacetylene chemistry the predictions appear to be reasonable. C_4H_4 profiles are fairly well reproduced by the model. However ethylbenzene and styrene concentrations are underpredicted whereas xylene concentrations are overpredicted by the model.

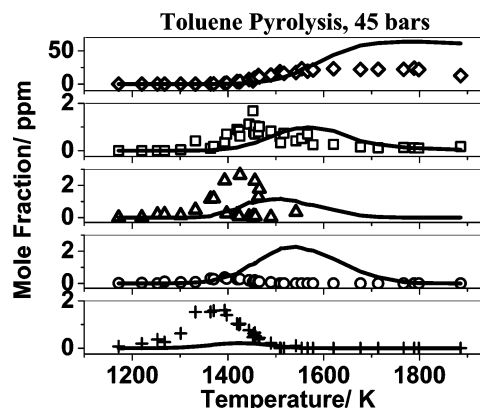


Figure 5. HPST profiles: (\diamond) C_4H_2 ; (\square) C_4H_4 ; (Δ) C_8H_8 ; (\circ) p -xylene; (+) ethylbenzene; (—) detailed model from Table ST2, part 1.

We have also estimated thermochemistry for the smaller aromatics and radicals in the model specifically for species not included in current databases^{26,27} such as the C_9H_9 isomers based on low level DFT methods (B3LYP/6-31G(d)) as implemented in the Gaussian 98²⁸ suite of programs by employing the methodology of ring-conserved isodesmic reactions^{29a,b} that use benzene and the smaller hydrocarbon molecules CH_4 , CH_3 , C_2H_6 , C_2H_4 and C_2H_2 as reference species for estimating heats of formation (ΔH_f^0 , 298 K). Table 2 is a compilation of the thermodynamic parameters for the small aromatic species in the model.

Conclusions

The pyrolysis of toluene has been studied at reflected shock pressures of 27 and 45 bar in the single pulse shock tube over the temperature range 1200–1900 K. A detailed model consisting of 262 reactions and 87 species assembled in part 1 of this series to validate the high-pressure limiting rate coefficients for the primary steps in toluene decomposition has been used to

TABLE 2: Thermochemistry

species	ΔH_f^0 (kcal/mol)	S_{298K} (cal/(mol K))
C ₆ H ₅	78.6 ^{1,30}	69.38 ³¹
C ₆ H ₆	19.85 ²⁷	64.48 ²⁷
C ₆ H ₅ CH ₂	51.50 ^{1,10}	76.04 ³²
C ₆ H ₅ CH ₃	11.95 ²⁷	76.52 ²⁷
p-C ₆ H ₄ CH ₃	71.80 ^{p.w.}	80.93 ^{p.w.,a}
C ₈ H ₆	78.44 ²⁷	78.36 ²⁷
C ₆ H ₅ CHCH	92.66 ^{29b}	82.28 ^{p.w.,a}
C ₆ H ₅ CCH ₂	81.99 ^{p.w.}	83.61 ^{p.w.,a}
C ₈ H ₈	35.49 ²⁷	82.58 ²⁷
C ₆ H ₅ CHCH ₃	41.84 ^{29b}	86.20 ^{p.w.,a}
C ₆ H ₅ CH ₂ CH ₂	57.60 ^{29b}	87.85 ^{p.w.,a}
p-xylene	4.28 ²⁶	92.89 ^{p.w.,a}
ethylbenzene	7.21 ²⁷	86.39 ²⁷
CH ₃ C ₆ H ₄ CH ₂	41.34 ^{29b}	87.65 ^{p.w.,a}
C ₉ H ₈	39.22 ²⁷	80.25 ^{p.w.,a}
s-C ₉ H ₈	68.54 ^{p.w.}	87.67 ^{p.w.,a}
t-C ₉ H ₈	73.52 ^{p.w.}	90.73 ^{p.w.,a}
p-C ₉ H ₉	92.12 ^{p.w.}	90.90 ^{p.w.,a}
c-C ₉ H ₉	72.10 ^{p.w.}	82.86 ^{p.w.,a}
i-C ₉ H ₉	87.97 ^{p.w.}	91.54 ^{p.w.,a}
s-C ₉ H ₉	50.24 ^{p.w.}	84.23 ^{p.w.,a}
n-C ₉ H ₉	92.71 ^{p.w.}	91.22 ^{p.w.,a}
f-C ₉ H ₉	86.49 ^{p.w.}	88.18 ^{p.w.,a}
pc-C ₉ H ₉	63.45 ^{p.w.}	87.19 ^{p.w.,a}
R1C ₉ H ₉	82.41 ^{p.w.}	92.08 ^{p.w.,a}
R2C ₉ H ₉	80.33 ^{p.w.}	91.24 ^{p.w.,a}
R3C ₉ H ₉	87.50 ^{p.w.}	89.38 ^{p.w.,a}
R4C ₉ H ₉	88.45 ^{p.w.}	90.07 ^{p.w.,a}
R13C ₉ H ₉	87.03 ^{p.w.}	90.09 ^{p.w.,a}
R22C ₉ H ₉	60.78 ^{p.w.}	84.03 ^{p.w.,a}
C ₁₀ H ₈	35.98 ²⁷	79.64 ²⁷

^a Based on DFT [B3LYP/6-31G(d)] structures.

simulate the formation of the observed key soot precursor intermediates. Because of its presence in significant amounts in the current experiments the decomposition of the benzyl radical is responsible for the growth of key soot precursors such as acetylene and indene. Mechanistic routes for the decay of the benzyl radical as well as the formation of key soot precursor species were tested. The assembled detailed model is able to explain the decay of benzyl from recent high-temperature experiments as well as the subsequent growth of key soot precursors observed in the current high-pressure experiments.

Acknowledgment. Support for this research was provided by the Office of Basic Energy Sciences, Chemical Sciences Division, U.S. Department of Energy, through Grant No. DE-FG0298ER14897. Support for R.S.T. was provided under the auspices of the Office of Basic Energy Sciences, Division of Chemical Sciences, Geosciences and Biosciences, U. S. Department of Energy, under Contract No. W-31-109-ENG-38.

Supporting Information Available: Table ST1, a compilation of the molecular structures for the C₉ species used in the detailed model. This material is available free of charge via the Internet at <http://pubs.acs.org>.

References and Notes

- (1) Sivaramakrishnan, R.; Tranter, R. S.; Brezinsky, K. *J. Phys. Chem. A* **2006**, *110*, 9388–9399.
- (2) Smith, R. D. *Combust. Flame* **1979**, *35*, 179.
- (3) Smith, R. D. *J. Phys. Chem.* **1979**, *83*, 1553–1563.
- (4) Pamidimukkala, K. M.; Kern, R. D.; Patel, M. R.; Wei H. C.; Kiefer, J. H. *J. Phys. Chem.* **1987**, *91*, 2148–2154.
- (5) Colket, M. B.; Seery, D. J. *Proc. Comb. Inst.* **1994**, *25*, 883–891.
- (6) Braun-Unkhoff, M.; Frank, P.; Just, T. H. *Proc. Comb. Inst.* **1988**, *22*, 1053–1061.
- (7) Eng, R. A.; Gebert, A.; Goos, E.; Hippler, H.; Kachiani, C. *Phys. Chem. Chem. Phys.* **2002**, *4*, 3989–3996.
- (8) Klippenstein, S. J.; Harding, L. B.; Georgievskii, Y. Submitted for publication in *Proc. Combust. Inst.* **2006**.
- (9) Jones, J.; Backsay, G. B.; Mackie, J. C. *J. Phys. Chem. A* **1997**, *101*, 7105–7113.
- (10) Braun-Unkhoff, M.; Frank, P.; Just, T. H. *Ber. Bunsen-Ges. Phys. Chem.* **1990**, *94*, 1417–1425.
- (11) Hippler, H.; Reihs, C.; Troe, J. Z. *Phys. Chem., Neue Folge* **1990**, *167*, 1–16.
- (12) Oehlschlaeger, M. A.; Davidson, D. F.; Hanson, R. K. *J. Phys. Chem. A* **2006**, *110*, 6649–6653.
- (13) Frochtenicht, R.; Hippler, H.; Troe, J.; Toennies, J. P. *J. Photochem. Photobiol. A: Chem.* **1994**, *80*, 33–37.
- (14) Laskin, A.; Lifshitz, A. *Proc. Combust. Inst.* **1998**, *27*, 313–320.
- (15) Kern, R. D.; Zhang, Q.; Yao, J.; Jursic, B. S.; Tranter, R. S.; Greybill, M. A.; Kiefer, J. H. *Proc. Combust. Inst.* **1998**, *27*, 143–150.
- (16) Bockhorn, H.; Fetting, F.; Wenz, H. W. *Ber. Bunsen-Ges. Phys. Chem.* **1983**, *87*, 1067–1425.
- (17) Frenklach, M.; Clary, D. W.; Gardiner, W. C.; Stein, S. E. *Proc. Combust. Inst.* **1984**, *20*, 887–901.
- (18) Tokmakov, I. V.; Lin, M. C. *J. Am. Chem. Soc.* **2003**, *125*, 11397–11408.
- (19) Richter, H.; Mazyar, O. A.; Sumathi, R.; Green, W. H.; Howard, J. B.; Bozzelli, J. W. *J. Phys. Chem. A* **2001**, *105*, 1561–1573.
- (20) Heckmann, E.; Hippler, H.; Troe, J. *Proc. Combust. Inst.* **1996**, *26*, 543–550.
- (21) Lindstedt, P.; Maurice, L.; Meyer, M. *Faraday Discuss.* **2001**, *119*, 409–432.
- (22) Vereecken, L.; Peeters, J.; Bettinger, H. F.; Kaiser, R. I.; Schleyer, P. v. R.; Schaefer, H. F., III. *J. Am. Chem. Soc.* **2002**, *124*, 2781–2789.
- (23) Vereecken, L.; Bettinger, H. F.; Peeters, J. *Phys. Chem. Chem. Phys.* **2002**, *4*, 2019–2027.
- (24) Vereecken, L.; Peeters, J. *Phys. Chem. Chem. Phys.* **2003**, *5*, 2807–2817.
- (25) *Computational thermochemistry: prediction and estimation of molecular thermodynamics*; Irikura, K. K., Frurip, D. J., Eds.; American Chemical Society: Washington, DC, 1998.
- (26) Afeefy, H. Y.; Liebman, J. F.; Stein, S. E. *Neutral Thermochemical Data in NIST Chemistry WebBook*; NIST Standard Reference Database Number 69; Linstrom, P. J., Mallard, W. G., Eds.; National Institute of Standards and Technology: Gaithersburg, MD, March 2003; <http://webbook.nist.gov>.
- (27) Burcat, A.; Ruscic, B. Ideal Gas Thermochemical Database with updates from Active Thermochemical Tables. <ftp://ftp.technion.ac.il/pub/supported/aetdd/thermodynamics>; 16 Sep 2005. Mirrored at <http://garfield-chem.elte.hu/Burcat/burcat.html>; 16 Sep 2005.
- (28) Frisch, M. J.; Trucks, G. W.; Schlegel, H. B.; Scuseria, G. E.; Robb, M. A.; Cheeseman, J. R.; Zakrzewski, V. G.; Montgomery, J. A., Jr.; Stratmann, R. E.; Burant, J. C.; Dapprich, S.; Millam, J. M.; Daniels, A. D.; Kudin, K. N.; Strain, M. C.; Farkas, O.; Tomasi, J.; Barone, V.; Cossi, M.; Cammi, R.; Mennucci, B.; Pomelli, C.; Adamo, C.; Clifford, S.; Ochterski, J.; Petersson, G. A.; Ayala, P. Y.; Cui, Q.; Morokuma, K.; Rega, N.; Salvador, P.; Dannenberg, J. J.; Malick, D. K.; Rabuck, D.; Raghavachari, K.; Foresman, J. B.; Cioslowski, J.; Ortiz, J. V.; Baboul, A. G.; Stefanov, B. B.; Liu, G.; Liashenko, A.; Piskorz, P.; Komaromi, I.; Gomperts, R.; Martin, R. L.; Fox, D. J.; Keith, T.; Al-Laham, M. A.; Peng, C. Y.; Nanayakkara, A.; Challacombe, M.; Gill, P. M. W.; Johnson, B.; Chen, W.; Wong, M. W.; Andres, J. L.; Gonzalez, C.; Head-Gordon, M.; Replogle, E. S.; Pople, J. A. *Gaussian 98*, Revision A.11.3; Gaussian, Inc.: Pittsburgh, PA, 2002.
- (29) (a) Sivaramakrishnan, R.; Tranter, R. S.; Brezinsky, K. *J. Phys. Chem. A* **2005**, *109*, 1621–1628. (b) Sivaramakrishnan, R.; Tranter, R. S.; Brezinsky, K. *Proceedings of the Fourth Joint Meeting of the U. S. Sections of the Combustion Institute*; Combustion Institute: Philadelphia, PA, 2005.
- (30) McMillen, D. F.; Golden, D. M. *Annu. Rev. Phys. Chem.* **1982**, *33*, 493–532.
- (31) Janoschek, R.; Rossi, M. J. *Int. J. Chem. Kinet.* **2002**, *34*, 550–560.
- (32) Ruscic, B.; Boggs, J. E.; Burcat, A.; Csaszar, A. G.; Demaison, J.; Janoschek, R.; Martin, J. M. L.; Morton, M.; Rossi, M. J.; Stanton, J. F.; Szalay, P. G.; Westmoreland, P. R.; Zabel, F.; Berces, T. *J. Phys. Chem. Ref. Data* **2005**, *34*, 573–656.